Aging of polymers of intrinsic microporosity tracked by methanol vapour permeation

www.elsevier.com/locate/memsci

Aging of polymers of intrinsic microporosity tracked by methanol vapour permeation

Kryštof Pilnáček, Ondřej Vopička, Marek Lanč, Marcela Dendisová, Miroslav Zgažar, Peter M. Budd, Mariolino Carta, Richard Malpass-Evans, Neil B. McKeown, Karel Friess.

PII: S0376-7388(16)31431-4
DOI: http://dx.doi.org/10.1016/j.memsci.2016.08.054
Reference: MEMSCI14704

To appear in: *Journal of Membrane Science*

Received date: 13 April 2016
Revised date: 27 July 2016
Accepted date: 26 August 2016

Cite this article as: Kryštof Pilnáček, Ondřej Vopička, Marek Lanč, Marcela Dendisová, Miroslav Zgažar, Peter M. Budd, Mariolino Carta, Richard Malpass Evans, Neil B. McKeown and Karel Friess., Aging of polymers of intrinsic microporosity tracked by methanol vapour permeation, *Journal of Membran Science,* http://dx.doi.org/10.1016/j.memsci.2016.08.054

Aging of polymers of intrinsic microporosity tracked by methanol vapour permeation

Kryštof Pilnáček[a], Ondřej Vopička[a], Marek Lanč[a], Marcela Dendisová[a], Miroslav Zgažar[b], Peter M. Budd[c], Mariolino Carta[d], Richard Malpass-Evans[d], Neil B. McKeown[d], Karel Friess[a*]

[a]University of Chemistry and Technology Prague, Department of Physical Chemistry, Technická 5, Prague 6, 166 28, Czech Republic

[b]University of Chemistry and Technology Prague, Department of Mathematics, Studentská 6, Prague 6, 166 28, Czech Republic

[c]School of Chemistry, The University of Manchester, Manchester, M13 9PL, UK

[d]School of Chemistry, University of Edinburgh, Joseph Black Building, West Mains Road, Edinburgh EH9 3JJ, UK

[*]Corresponding author, Tel.: +420 220 444 029, E-mail: karel.friess@vscht.cz.

Abstract

The initially very promising transport properties of glassy high free volume polymers deteriorate rapidly over time. In this work, we focused on this aging phenomenon in two polymers of intrinsic microporosity (PIMs), namely PIM-1 and PIM-EA-TB. To identify the main mechanisms involved, we studied the time-declines of permeability and diffusivity of methanol vapours in flat membranes with approximately equal thicknesses. The permeation measurements were carried out using a continuous flow permeation method with carrier gas, where the methanol vapours were held at constant activity 0.2 at 25°C. Two different experimental modes were used: (i) continuous experiments that consisted of one long experiment with a duration of over 650 hours for each polymer and (ii) momentary experiments that consisted of a vast number of short (*ca.* 6 hours) consecutive measurements of transient permeation. The observed decreases of methanol permeability due to aging were more intense in the case of continuous mode for both polymers. In other words, the aging was *ca.* 1.3 times faster in the continuous mode in comparison with the

momentary mode. Using time-aging time superposition, we successfully predicted the continuous experiments from the momentary experiments.

Keywords: Polymer of intrinsic microporosity, aging, infrared spectroscopy, methanol vapour permeation

Nomenclature

Roman symbols

A	active surface of the membrane
a	activity
c	molar concentration
f	heat of adsorption of the sorbate from the bulk phase to the second and higher monolayers
D	diffusion coefficient
$\mathfrak{D}$	thermodynamic diffusion coefficient
h	heat of adsorption of the sorbate from the bulk phase to the first monolayer
H	mobility coefficient of the diffusing molecules
j	molar flow of vapours
J	flux of vapours
k	adjustable parameter in Eq. (2)
L	thickness of a membrane
M	mobility of polymer chains
$\dot{n}$	molar flow
p	pressure
P	permeability
r	correlation coefficient
$\mathbf{R}$	universal gas constant

S	sorption coefficient
t	time
T	thermodynamic temperature
v	sorption capacity of sorbent (in units gpenetrant/gpolymer)
w	weight fraction of vapours
x	molar fraction of vapours
z	position in membrane

Greek symbols

α	vertical shift factor
θ	effective time
μ	double-logarithmic shift rate, defined by Eq. (8) in [36], or ,in Appendix, chemical potential
ϕ	volume fraction of vapours

Subscripts

atm	atmospheric
carr	carrier gas
feed	feed/retentate/upstream part of a measuring cell
m	first adsorption monolayer
mol	molar
perm	permeate/downstream part of a measuring cell
ref	reference
sat	saturated vapour (used in connection with presure)
STP	standard temperature and pressure (273.15 K, 101.325 kPa)
st	steady state
vol	volumetric
w	elapsed from the start of aging (used only in connection with time)

1 Introduction

The polymers of intrinsic microporosity (PIMs) represent a novel class of the glassy high free volume polymers. Thanks to their high permeabilities and moderate selectivities, PIMs exhibit very good perm-selective properties [1]. Recently, several PIMs have overcome Robeson's 2008 upper bound [2] for certain pairs of gases [3-6]. This achievement makes PIMs potentially very attractive for industrial use. However, PIMs also exhibit two quite challenging issues. The first one is their very complex transport behaviour [7]. For example, their transient sorption kinetics cannot be described by the commonly used Fick's second law of diffusion. The second problem is the aging phenomenon [8], which causes a significant decrease of PIMs permeability over time [3, 6, 9-13].

The first issue can be addressed using non-Fickian models, for instance see literature [14-21]. As a first approximation, we used an improved Fick's law with activity corrected diffusion coefficient, which is also known as the thermodynamic Fick's law [19-22]. For more insight into the derivation of the thermodynamic Fick's law, see Appendix A.1.

$$J_{\mathrm{vol}} = -\mathfrak{D} \cdot \left(\phi \frac{\partial \ln a}{\partial \phi}\right) \frac{\partial \phi}{\partial z} \qquad (1)$$

The Eq. (1) provided an improved description of the transient permeation kinetics in comparison with the plain Fick's law. A more detailed study on this topic could provide some insight into the polymer, which is of interest in the academic point of view. We, however, focused on the aging phenomenon, which is of major concern from the industrial point of view.

It was shown in recent works [23-27] that PIMs aging can be tackled using organic additives such as porous organic molecular crystals [28] (cages), porous aromatic frameworks [29] (PAFs) [28]or hypercrosslinked polystyrene fillers [27] (HCP). The decline of material permeability was lower than 10% of the initial permeability over one year for PIM-1 membrane with PAFs [25], lower than 60% for PIM-1 with cages [26] and about 40% over half a year for PIM-1 with HCP [27] , while the usual decline over one year is about 70% [26]. Furthermore, an increase in absolute permeability was observed for all the types of additives [27]. Thus, such an approach represents a convenient way to mitigate the effect of aging and even improve the membrane separation properties [24]. Despite all this progress, there are still some missing pieces in the puzzle of aging of PIMs, such as the influence of the permeating compounds. To explore the aging phenomenon, various authors use different methods to monitor the aging of polymeric membranes. Some studies were focused on changes in the physical structures of polymers, detected using SAXS/WAXS [12] or PALS [9, 30], while others were focused on the influence of aging on the permeability [10, 11, 30-32]. Furthermore, theoretical

computation methods [13] were reported as well. However, only a few of the aforementioned studies mention the aging phenomenon in PIMs [9-12]. Moreover, to the best of our knowledge, there are neither studies about the nature (chemical or physical) of aging of PIMs, nor on the influences of the permeating compounds.

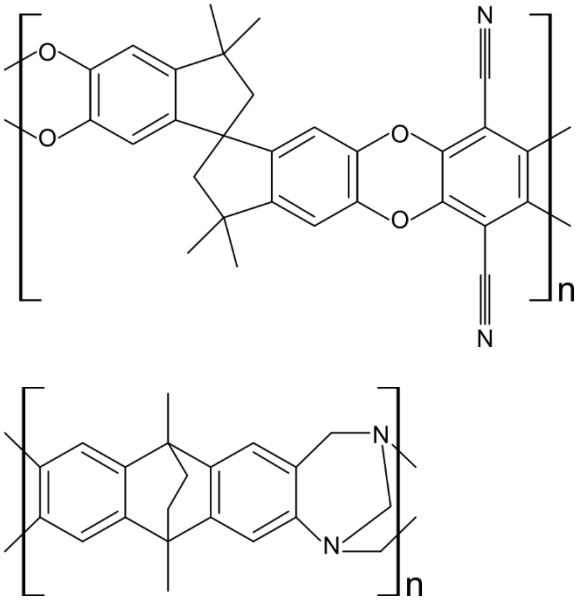

Figure 1 – Schematic structures of studied polymers: PIM-1 (upper), PIM-EA-TB (lower).

In this work, PIM-1 [3] and PIM-EA-TB [5] (see Figure 1) were chosen from the family of polymers of intrinsic microporosity. PIM-1 is an archetypal polymer, which was the first prepared PIM and is currently the most studied one [3, 7, 9-12, 33-35]. PIM-EA-TB was chosen because of its unique properties, especially for its gas separation ability [5]. To the best of our knowledge, the aging of PIM-EA-TB has not yet been systematically studied, with a few basic details described in the literature [5, 6].

To the best of our knowledge, the aging measurements are commonly carried out only by measuring a series of consecutive short-term measurements, for examples see [10, 24-26, 31, 32]. Moreover, the measurement protocols are far from being comparable (time intervals between two consecutive measurements differ widely). On the other hand, in the industrial applications, the membrane separation processes run continuously for months. Struik [36] described significant differences

between these two modes of measurements for the rheological behaviour of polymeric materials. In this study, we thus focused on the comparison of these two modes of measurement.

At first, we used infrared transmission spectra to validate the assumption that PIMs undergo only the physical aging. Then, methanol (MeOH) vapour permeability experiments were performed using a flow permeameter with carrier gas (often referred to as Wicke-Kallenbach technique). This apparatus was used because (i) it provides stable boundary conditions, (ii) the studied membrane is under no mechanical stress and (iii) it enables continuous long-term permeation tests to be performed as well as the short-term ones. The measurements were carried out in two different modes: continuous mode (one experimental run lasted more than 650 hours) and momentary mode (numerous short-term experimental runs, each of which lasted about 6 hours). Moreover, as the measurements were conducted using MeOH vapours, long-term effects similar to that of the so called MeOH treatment [6] can be expected and were, indeed, also observed in this work.

The principal aim of this study is to improve understanding of the time-dependent transport properties of the PIM-1 and PIM-EA-TB with the following objectives: (i) to validate the assumption of physical aging of PIMs; (ii) to elucidate the rate of the aging process under different measurement conditions (comparison of the momentary and the continuous modes) and thus to detect if there is a contribution of the permeating compound; (iii) to identify whether the decline of permeability is caused by the changes in diffusion coefficient or sorption coefficient; and (iv) to predict the continuous permeation behaviour of PIM membranes using correlative models.

1.1 Theoretical treatment of physical aging

Although the aging process can be caused by several different chemical or physical processes, the most important one and possibly the only one occurring in PIMs is the physical aging. Thus, theoretical backgrounds of physical aging are given here.

The physical aging of glassy polymers was thoroughly studied by Struik [36]. This author described short-term (momentary) rheological measurements of glassy polymers and from these predicted the long-term (continuous) behaviour of polymers. He concluded that a glassy polymer exposed to a constant long-term stress ages much slower in comparison to a situation when it is under periodically applied short-term stresses. This effect is very beneficial and allows glassy polymers to be used, for instance, as building materials.

For the prediction, Struik used time-aging time superposition in the effective time domain. This approach was improved in more recent studies by Joshi *et al.* [37, 38]. Moreover, Joshi *et al*. studied not only the rheological properties of glassy polymers but also properties related to polarization (see

Figure 11 in literature [38]). These authors concluded that their approach can be used to model, in principle, any time dependent process in polymers. Thus, we used their approach to predict the polymer aging connected with the decline of material permeability in continuous mode from the experimental data obtained in momentary mode.

[36][37][39][40]Further, an alternative approach to the description of physical aging in glassy polymers was reported by Zhou *et al*. [41]. They used the following equation for the description of aging:

$$\ln P = k_1 - k_2 \ln t \quad (2)$$

Both parameters are adjustable, positive, temperature dependent and possess some physical meaning. The parameter k_1, as Zhou stated, possibly corresponds to the logarithm of approximate reference starting value of permeability during the aging process [41]. Thus, k_1 is not very important for this study. Parameter k_2 corresponds to the rate of aging at a temperature below the glass transition [41], which can be used for the comparison of aging rates of the studied polymers. The most important benefits of this equation are its simplicity and applicability to quite a long time range of data. Interestingly, as Eq. (2) does not explicitly involve any free volume characteristics of the polymer, this model can be utilized even if these characteristics are not known. However, a relation of parameter k_2 to the rate of contraction of free volume of the polymer can indeed be expected.

2 Experimental part

2.1 Chemicals

The chemicals used for the permeation experiment were MeOH (Penta, min. 99.8%) as a penetrant, chloroform stabilized with amylene (Lach-ner, 99.88%) as a solvent, hydrogen (SIAD Czech, 99.9995%) and helium (SIAD Czech, 99.998%) as the carrier gases. All chemicals were used without further purification.

2.2 Membrane preparation

Polymers were prepared according to the procedures previously described in [5, 42] for PIM-EA-TB and [43] for PIM-1. Thin flat membrane samples were prepared by the solvent evaporation method from 2 – 3 wt.% polymer solutions in chloroform and dried in partially covered Petri-dishes under ambient temperature and pressure for at least 12 h. In order to remove the residual solvent (for details see Appendix A.2 for PIM-1 and the literature [6] for PIM-EA-TB) and to rejuvenate the polymer structure, the as-cast films were treated with liquid MeOH. The treatment was performed by immersing the membrane overnight in MeOH and then allowing it to dry for 1 h under ambient

conditions. Then the membrane was then placed into a permeameter, where it stayed another *ca*. 2 h under pure carrier gas, whose continuous streams were conducted to both sides of the membrane, as the used type of detector needs this period of time to stabilize its signal. In order to obtain aged samples, two different membranes were kept overnight at a temperature of 125 °C (in air); thus, so called thermally-aged (annealed) samples were obtained. The thicknesses of studied membranes were determined by a dial comparator (Somet) and are stated in Table 1. Additionally, this table contains the type of permeation experiment for which each membrane was used.

Table 1 – A list of samples, their thicknesses (measured after MeOH treatment) and the mode of experiment in which they were used

Material	Thickness (μm)	Type of experiment
PIM-1	241±4	Momentary
PIM-1	183±5	Continuous
PIM-EA-TB	147±4	Momentary
PIM-EA-TB	152±7	Momentary
PIM-EA-TB	123±4	Continuous

2.3 Infrared spectroscopy

The infrared (IR) transmission analysis of as-cast and MeOH treated samples was done using a NICOLET 670 FTIR spectrometer (Thermo Fisher Scientific Inc.) equipped with a transmission accessory (Thermo Fisher Scientific Inc.). A heated ceramic (Globar) source of infrared beam, KBr beam splitter and DTGS (Deuterated TriGlycin Sulfate) detector were used in this setup. The spectra were collected in the range 4000 – 400 cm^{-1} and evaluated in Omnic software. A total of 64 scans at a resolution of 2 cm^{-1} were recorded for each spectrum.

IR surface analysis of samples kept at 25°C and of thermally aged samples was carried out using a NICOLET IS-50 FTIR spectrometer (Thermo Fisher Scientific Inc.) equipped with a built-in diamond ATR sampling station (Thermo Fisher Scientific Inc.). Polaris™ source of infrared beam, KBr beam splitter and Dedicated DLaTGS (Deuterated Lanthanum α Alanine doped TriGlycine Sulphate) detector were used in this setup. The spectra were collected in the range 4000 – 400 cm^{-1} and evaluated in Omnic software. A total of 64 scans at a resolution of 2 cm^{-1} were recorded for each spectrum.

2.4 Permeation experiment

The permeation experiments were carried out using a continuous flow permeameter [44-46], for detailed scheme see Figure 2. The measuring cell of this apparatus is divided into two parts by the

tested flat sheet membrane. The upper part is in contact with the gas mixture of exactly defined degree of saturation maintained at atmospheric pressure. The lower part is in contact with the pure carrier gas which sweeps permeate from the cell and is maintained at atmospheric pressure. The resulting permeate mixture is then analysed using a thermal conductivity detector (TCD), for which hydrogen and helium are common carrier gases.

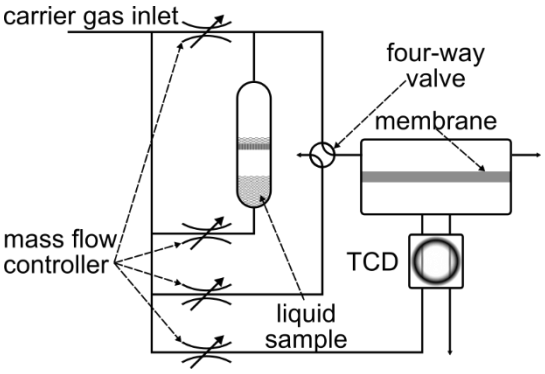

Figure 2 – Schematic diagram of differential flow permeameter. TCD – thermal conductivity detector.

Hydrogen and helium were used as the carrier gases because of their high thermal conductivity. For frequent short measurements hydrogen was used, because it is cheaper, and for the long-term (non-stop) experiments helium was used in order to avoid any dangerous situations connected with potential leaking of flammable explosive hydrogen during periods with no attendance of researchers in lab. The carrier gas was fed into the mass flow controller (MFC, producer Aalborg). One stream of carrier gas was led from the MFC into a double-jacketed saturator maintained at (25.0±0.1) °C using a circulation bath (Huber ministat 125), where it was saturated with the vapours of MeOH. The resulting stream of the fully saturated carrier gas was then diluted with the pure carrier gas, to a set MeOH concentration (and thus MeOH vapour activity). Such mixture was led to the upstream part of the cell. The measuring cell was thermostated at (25.0±0.1) °C using the same circulation bath (Huber ministat 125). Because the signal of TCD is sensitive to temperature disturbances, the whole apparatus (except computer) was enclosed in a thermostated air box (29.8±0.1) °C. All temperatures were checked using a platinum resistivity thermometer (Pt 100-Testo 735-2).

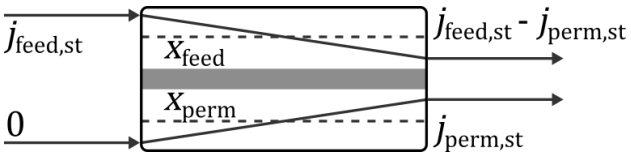

Figure 3 – Mass balance schema for correction of boundary conditions

This setup ensures stable boundary conditions at both sides of the membrane. However, the upstream concentration is lowered and the downstream concentration is increased (see Figure 3) by the vapour flux through the membrane, when compared to a (very) low permeable membrane. Thus,

as a first approximation, the concentration in the upstream part equals the set MeOH concentration in the feed mixture and in the downstream part equals zero. As PIMs are highly permeable membranes, corrections devised from mass balance were used [44] (for details see Figure 3). The corrections were estimated using the following equations

$$x_{\mathrm{feed}} = \frac{\left[j_{\mathrm{feed,st}} + \left(j_{\mathrm{feed,st}} - j_{\mathrm{perm,st}}\right)\right]/_2}{\left[j_{\mathrm{feed,st}} + \left(j_{\mathrm{feed,st}} - j_{\mathrm{perm,st}}\right)\right]/_2 + \dot{n}_{\mathrm{carr,feed}}}, \tag{3}$$

$$x_{\mathrm{perm}} = \frac{j_{\mathrm{perm,st}}/_2}{j_{\mathrm{perm,st}}/_2 + \dot{n}_{\mathrm{carr,perm}}}. \tag{4}$$

Permeability coefficients were calculated from Fick's first law

$$P = \frac{L}{p_{\mathrm{atm}}\left(x_{\mathrm{feed}} - x_{\mathrm{perm}}\right)} \frac{j_{\mathrm{perm,st}}}{A} \frac{\mathbf{R}\, T_{\mathrm{STP}}}{p_{\mathrm{STP}}}, \tag{5}$$

where $j_{\mathrm{perm,st}}$ is molar flow of vapours in steady state in the lower part of the cell. This quantity was obtained from the calibration of the TCD, whose signal is proportional to this quantity. The calibration was carried out by weighing the permeate condensed in a liquid nitrogen cold trap [47] over a certain period of time. The weighing was carried out using the Ohaus DV215CD laboratory balance.

In order to assess the diffusion coefficients of momentary experiments, the thermodynamic Fick's diffusion flux Eq. (1) was used together with the sorption model named after Guggenheim, Anderson and de Boer, which is usually abbreviated as the GAB model [7, 48-50]. The thermodynamic Fick's second law then has the form

$$\frac{\partial \phi}{\partial t} = \frac{\partial}{\partial z}\left[\mathfrak{D} \cdot \left(\phi \frac{\partial \ln a}{\partial \phi}\right) \frac{\partial \phi}{\partial z}\right]. \tag{6}$$

In Eq. (6), the volume fractions ϕ were approximated by weight fractions w (the same way as in the literature [51]). Therefore, the GAB model was used in the following form:

$$w = \frac{v_{\mathrm{m}} h f a}{(1 - fa)(1 - fa + hfa) + v_{\mathrm{m}} hfa} \tag{7}$$

The term $\left(\phi \frac{\partial \ln a}{\partial \phi}\right)$ in Eq. (6), which describes the dependence of the overall diffusion coefficient on concentration, was obtained, keeping in mind the substitution $\phi = w$, from Eq. (7) in the following form:

$$\left(w\frac{\partial \ln a}{\partial w}\right) = \frac{v_{\mathrm{m}}h}{\sqrt{v_m^2h^2(1-w)^2+2v_{\mathrm{m}}h\,w(1-w)(2-h)+w^2h^2}} \tag{8}$$

In order to assess the improvement of the description of the transient permeation kinetics, we also computed diffusion coefficients using the plain Fick's second law [52]

$$\frac{\partial \phi}{\partial t} = D\frac{\partial^2 \phi}{\partial z^2}\,. \tag{9}$$

The boundary conditions, for Eqs. (6) and (9), were computed from Eq. (7). For the numerical computation, Python programming language and its libraries included in the scientific package Anaconda [53] were used. Space discretization of Eq. (6) was performed using linear finite element method on one dimensional mesh with non-equidistant spacing, which corresponded to Chebyshev nodes. Time discretization was performed using Sundials' solver IDA from the Python package Assimulo [54]. Finally, the model was fitted to the transient permeation data using the Nelder-Mead method and subsequently refined by the least-squares method, both from lmfit package [55].

When compared, Eq. (6) described all kinetic curves better than Eq. (9), as can be seen from Figure 4, Table A.1 and A.2. Moreover, the advanced diffusion model provided a more realistic non-linear steady state concentration profile (see Figure 10), in comparison with the classic Fickian behaviour. In fact, the concave tendency of non-linear steady state can possibly describe the inner swelling phenomena.

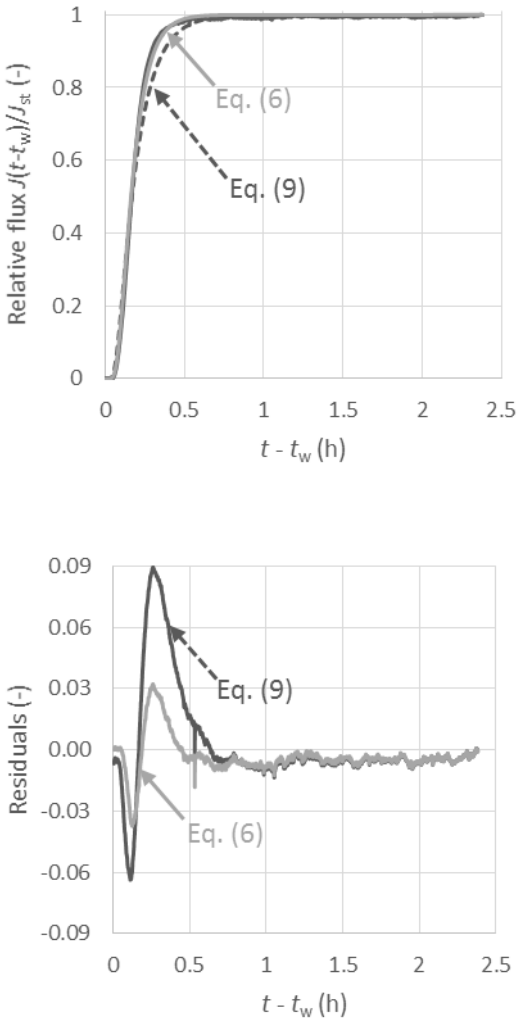

Figure 4 – Example of fitted experimental data (PIM-EA-TB, MeOH 20%, day 2) using Eq. (6) and Eq. (9) (upper plot) and the residuals between the experimental data and Eq. (6) and Eq. (9), respectively (lower plot). Adjusted R^2 are 0.998 for Eq. (6) and 0.989 for Eq. (9).

2.5 Sorption experiment

In order to assess the diffusion coefficient of Eq. (6), it was necessary to obtain coefficients of Eq. (7). The activity of MeOH vapors was estimated by the following equation.

$$a = {}^{p}/_{p^{\mathrm{sat}}} \tag{10}$$

For PIM-1, the coefficients were found in the literature [7]. Those for PIM-EA-TB were calculated from the experimentally determined sorption isotherm, which was measured using the same gravimetric apparatus and at the same conditions as in the literature [7]. Hence, we only state the resulting sorption plot (see Figure 5 and Table A.3) and the coefficients of Eq. (7) v_{m} = 0.237 ± 0.008 g/g, h = 23.7 ± 2.4, f = 0.628 ± 0.018. The sorption experiments were conducted within the course of 8 days, no changes of sorption uptake imposed by aging were observed by means of re-measuring

the point at α = 0.2, see Fig. 5. Similar time-invariability of sorption isotherms was also reported for PIM-1 [7, 56].

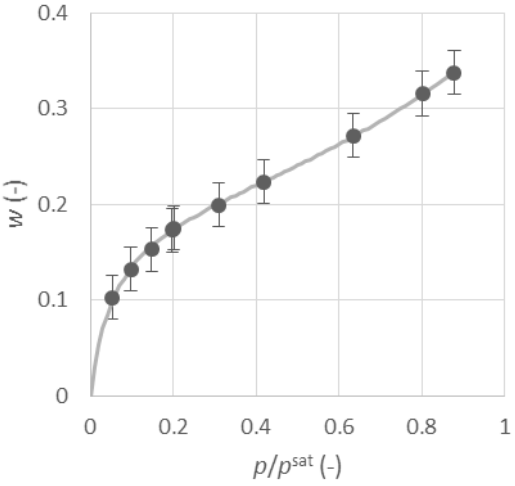

Figure 5 – Sorption isotherm of MeOH in PIM-EA-TB at 25°C. The experimental data (dots) were fitted with GAB model (solid line) Eq. (7).

3 Results and discussion

3.1 Chemical vs. physical aging

Aging of PIM-1 membrane, which was simulated by the thermal treatment (for more information see section 2.2), was studied using ATR-FTIR spectroscopy. Average spectra from two measurements of the membrane exposed to 25°C and to 125°C showed no distinguishable spectral differences in the chemical composition of the "new" membrane (presented by the temperature 25°C) and the "old" membrane (presented by the temperature 125°C).

A similar comparison was made also for a PIM-EA-TB membrane, where the average spectra (of the membrane exposed to 25°C and to 125°C) showed no distinguishable differences between the two spectra as well. For more details see the spectra in Supporting information (Figures S1 and S2).

The ATR-FTIR spectroscopy showed no distinguishable chemical changes between the new and the old membrane for both PIM-1 and PIM-EA-TB. Thus, it can be concluded that the physical aging, which is undetectable using IR spectroscopy, largely dominates the aging process in PIMs. Hence, in this work, the theoretical treatment of aging is focused only on the physical aging phenomenon.

3.2 Permeability and diffusivity decline

3.2.1 Aging in the momentary and continuous mode

During the continuous mode of measurement, strong declines of MeOH permeabilities were observed for both studied membranes (see Figure 6). PIM-1 exhibited lower initial permeability, but aged more slowly in comparison with PIM-EA-TB. More specifically, the parameter k_2 of Eq. (2) was roughly two times higher for PIM-EA-TB than for PIM-1 (see Table 2). This observation coheres with that observed in the literature [57]. The authors proposed an explanation that materials with stiffer polymer chains (PIM-EA-TB has stiffer chains than PIM-1 [5]) have higher initial permeability but age faster.

For both polymers, it was possible to clearly distinguish three stages of the diffusion process (see lower plot of Figure 6). In the first stage, ranging from the beginning to 0.6 hours, the transitional diffusion process took place. In this time range, diffusion started and reached steady state. In the second stage, ranging from 0.6 to 2 hours, the diffusion was in a normal steady state. In the last and longest stage, which started at about 2 hours, the long-term aging phenomenon occurred. In the log-log plot (lower plot of Figure 6), one can see that the aging slowly accelerated and reached steady exponential decrease at about 100 hours. Such aging should reach, according to Eq. (2), the permeability of 0 Barrer in infinite time.

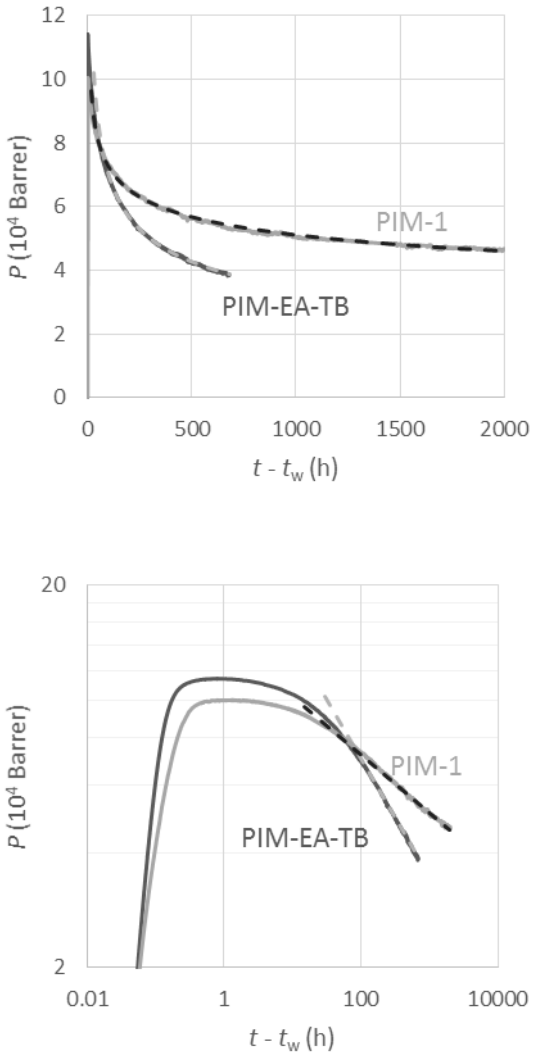

Figure 6 – Continuous aging experiments for PIM-1 and PIM-EA-TB membranes (MeOH activity 0.2, 25 °C) in linear (upper plot) and log-log (lower plot) scale. Both plots show the same data. Dashed lines are fitted using Eq. (2)

During the momentary mode of measurement, we observed a strong decline in transport properties that was very similar to that seen in the continuous mode (see Figure 7). However, for PIM-1 membrane, the momentary experiments departed from the exponential trend and stabilized at about 1000 hours (see upper plot in Figure 7). Moreover, such a disproportion was also noticeable for some other points (namely at 99, 267, 314, 795 and 2835 hours, see the encircled points in the upper plot of Figure 7), which appeared above the curve of continuous experiment. These experiments were carried out after a longer interval between the two consecutive measurements (Δt_w) than the other experiments (see Table A.1).

For PIM-EA-TB, the difference between the continuous and momentary mode was even more pronounced (see lower plot in Figure 7). These observations for both membranes indicate a negative dependence of aging on Δt_w; *i.e.* the longer the Δt_w is, the slower the aging is.

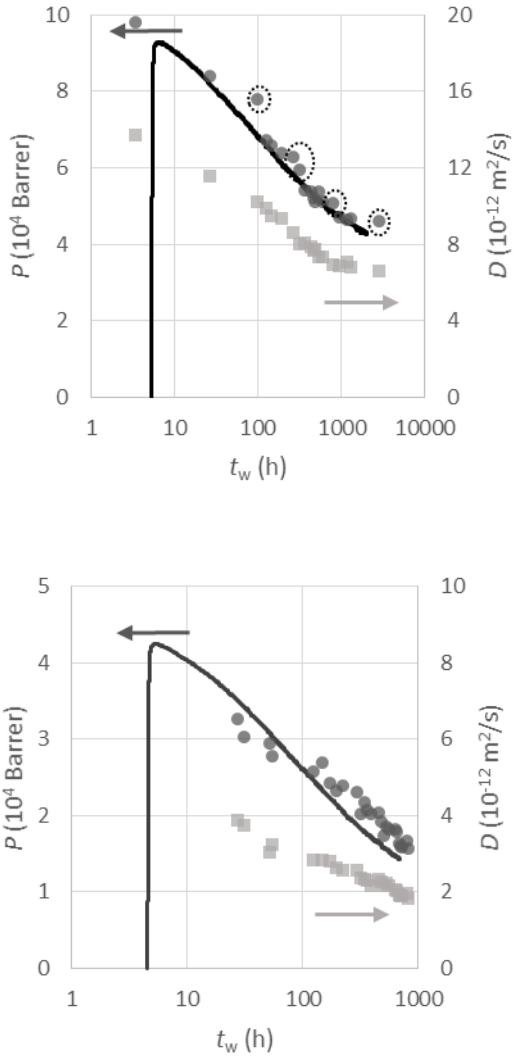

Figure 7 – Relative comparison of momentary (points) and continuous (line) experiments for PIM-1 (upper plot) and PIM-EA-TB (lower plot) membrane (MeOH activity 0.2). Permeabilities (left axis) were evaluated using Eq. (5) and diffusivities (right axis) using Eq. (6). The continuous measurements were adjusted to match the momentary data using Eq. (13) with α = 0.925 for PIM-1 and α = 0.372 for PIM-EA-TB.

In conclusion, from our observations it follows that the process of physical aging of polymers with intrinsic microporosity is faster in the continuous than in the momentary mode.

3.2.2 [37][37][58][59]Aging related to decline in diffusion coefficient

The third aim of this study was to look at the internal cause of aging. In other words, at the question of whether the decline in permeability (P) is caused by the decline of diffusion coefficient (D) or of sorption coefficient (S) or both. In Figure 7, the permeability and diffusivity coefficients appear to be very well correlated. This is also confirmed by a numerical evaluation of the correlation coefficient (r) between permeability and diffusivity. For PIM-1, r reached 0.973 and for PIM-EA-TB 0.961. In both cases, strong outliers were omitted (see the crossed values in Tables A.1 and A.2) and diffusion

coefficients obtained from Eq. (6) were used. Such a correlation supports the possibility that the decline in permeability could be caused only by the decline in diffusion coefficient.

This finding was supported by fitting Eq. (2) to the experimental data obtained during momentary experiments as well as by the repeatability of sorption tests (section 2.5). The fit was carried out for both the permeability and the diffusion coefficients. The resulting parameters k_2 are stated in Table 2.

Table 2 – Parameters k_2 of Eq. (2) evaluated for diffusion and permeability coefficients for both tested membranes.

	k_2(permeability, continuous)	k_2(permeability, momentary)	k_2(diffusivity, momentary)
PIM-1	0.152	0.136	0.128
PIM-EA-TB	0.312	0.205	0.198

From Table 2, one can see, that the rate of aging (parameter k_2) of permeability in momentary mode almost equals that of diffusivity; hence, we reach the same conclusion as in the previous paragraph: drop of permeability is governed only by the drop of diffusion coefficient.

Moreover, this conclusion was supported by the good reproducibility of the first and the last sorption point (see Figure 5 and Table A.3), which was re-measured at the same vapor activity after 193 hours of aging and rendered the same sorption uptakes (*i.e*. constant sorption coefficient). Constant sorption uptakes over more than 1000 days were also observed by other authors and a study on that topic is being prepared [56].

3.2.3 Prediction of permeability

For the prediction of continuous permeability data from the momentary experimental data, the procedure of Joshi *et al*. [37, 38] was used. Concretely, the approach used in the study of Joshi *et al*. consists of several steps. The experimental data obtained in momentary mode are transformed to the effective time domain θ using the following equation

$$\theta = \frac{t^{1-\mu} - {t_w}^{1-\mu}}{1-\mu}, \tag{11}$$

where t is the actual time of an experiment, t_w is the aging time (time since the last rejuvenation) and μ is double log shift rate

$$\mu = -\frac{\mathrm{d}\ln M}{\mathrm{d}\ln t_w} \tag{12}$$

as defined by Eq. (3) in [36], where M denotes mobility of polymeric chains and t_w has the same meaning as in Eq. (11). Thanks to this transformation, one can see the steady-state parts of each

momentary experiment no matter the length of experimental time nor the aging time (cf. upper and lower plot in Figure 8).

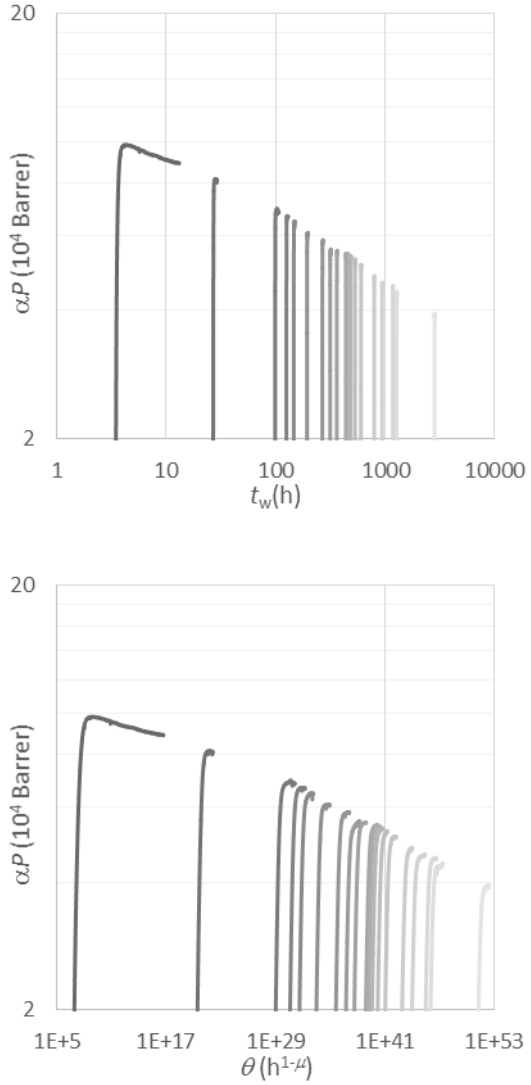

Figure 8 – Momentary data of PIM-1 with respect to aging time t_w (upper plot) and transformed into the effective time domain θ (lower plot).

After the transformation of permeability data into the effective time domain θ, it is possible to vertically shift the permeability signal using the following equation

$$P^* = \alpha \cdot P. \tag{13}$$

The parameters μ and α should be adjusted in such a way that the steady-state parts of consecutive momentary experiments lie on one smooth curve (so-called master curve). These adjustments are carried out in log-log coordinates. Subsequently, the master curve is used for the predictions of continuous permeabilities by the transformation from the effective time domain back to normal time using the following equation

$$t = [\theta \cdot (1-\mu) + {t_w}^{1-\mu}]^{1/1-\mu}, \quad (14)$$

where t_w is substituted with an aging time, from which we want to predict the continuous behaviour. For more details of this procedure see the literature [37, 38]. In this work, for the momentary experimental data obtained, the optimal value of parameter μ was found to be −15 for both studied membranes. The parameters α differed for each permeability experiment and are stated in Table A.1 for PIM-1 and Table A.2 for PIM-EA-TB.

If $\mu = -15$ is substituted into Eq. (12), an interesting paradox arises. With μ lesser then 0, the mobility M should *increase* as the polymer ages. This is in stark contrast with the theory of Struik, who states that with decreasing free volume the mobility should *decrease* over time [36]. A possible explanation to that observation could be in the different nature of processes observed in this work and by Struik. Struik observed creep compliance, which generally increases over the measurement time and decreases over aging time. However, permeability decreases over both the measurement time as well as the aging time. This could explain the opposite sign of μ than is expected from the Eq. (12) and not violate the assumption that M decreases over aging time. Generally, this could imply that permeability of any glassy polymer decreases *faster* in the continuous mode than in the momentary mode.

This procedure led to a very good agreement between the predicted (black solid line) and experimental (red solid line) continuous behaviour (see Figure 9).

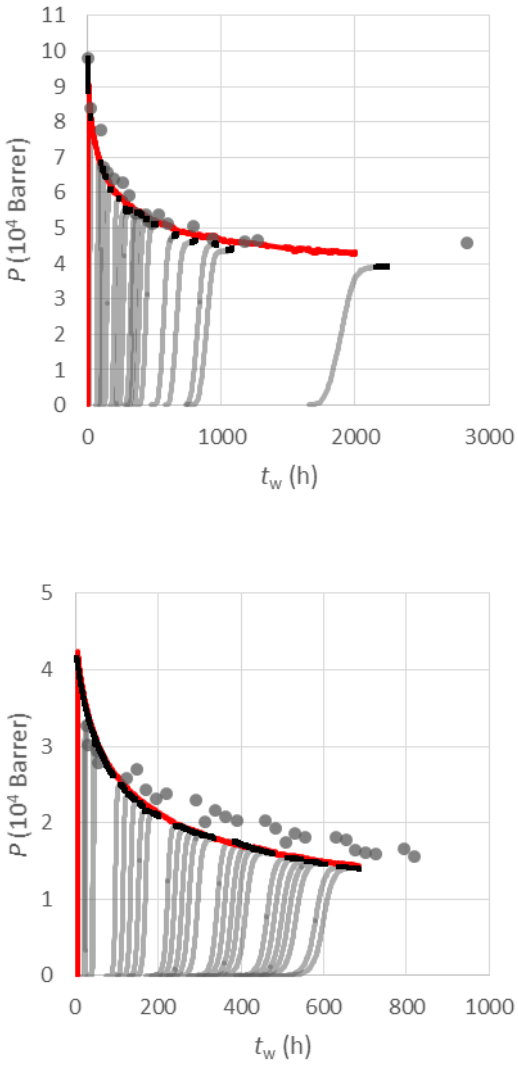

Figure 9 – Comparison of momentary experiments (grey dots), transformed momentary experiments (grey lines), predicted continuous experiments (black lines) and measured continuous experiments (red lines) for PIM-1 (upper plot) and PIM-EA-TB (lower plot).

The value of the parameter μ corresponds to the different regimes of aging. Values of μ equal to zero mean that there is no aging, μ being between zero and unity means the so called "sub-aging" [37], μ equal to unity mean regular aging, and values of μ greater than unity mean so called "hyper-aging" [37]. All of these values also mean that the continuous mode is beneficial for the material; *i.e.* aging is slower under continuous loading than under repeated momentary loadings. However, in the case of permeation, the trend seems to be quite the opposite. Thus, the opposite (negative) value of μ can be justified. The very high absolute value of μ indicates high sensitivity to the length of Δt_w.

Further evidence favouring the idea of some dependence of aging rate on Δt_w, was found in a correlation between α and Δt_w. For PIM-1, the correlation coefficient reached −0.470 and for PIM-EA-TB −0.555. In both cases, strong outliers were omitted (see the crossed values in Tables A.1 and A.2). This means the higher Δt_w, the more it was necessary to vertically adjust experimental curves.

As the last indication that aging in the continuous mode is *faster* than in the momentary mode, we compared the parameters k_2 of Eq. (2). For both tested membranes, k_2 reached higher values (faster aging) in the continuous mode (see Table 2) than in the momentary mode. Numerically, the aging was accelerated by *ca*. 1.3 times in the continuous mode.

The effect of continuous mode on permeation could be explained by the permanent presence of penetrant itself. MeOH readily swells both PIM-1 [58] and PIM-EA-TB [6]. In the swollen state, the polymer chains are probably much more mobile; thus, it is easier for them to move towards their equilibrium (aged) conformation. However, this is in strong contrast with the rejuvenation capability of the MeOH treatment [59]. This discrepancy could be caused by the difference in activities of MeOH. During the MeOH treatment, the membrane is immersed in liquid MeOH (a = 1), while during our permeation experiments the activity was around 0.2 on the upstream side of the membrane and decreased with the decreasing concentration throughout the membrane (see Figure 10). Thus, MeOH could probably not swell the polymer structure enough and only helped the polymer chains to reach more packed conformation.

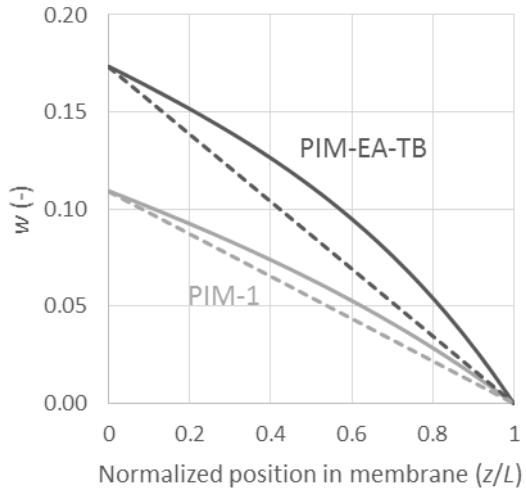

Figure 10 – Computed concentration profiles throughout the membranes in steady state. The computation was performed for MeOH using Eq. (9) (dashed line) and Eq. (6) (solid line), upstream activity 0.2, downstream activity 0.0, thickness 147 μm, and D = 4.0 10^{-12} m^2/s.

As the parameter μ is negative, the predicted continuous data describe shorter time interval than the original momentary data. Although this fact makes this procedure unusable for extrapolation, it is invaluable for the transformation of experimental data obtained in the momentary mode to continuous mode.

In order to extrapolate the experimental data in continuous mode, we used Eq. (2) (see Figure 11). Using the fitted parameters (see Table 2), we computed the time at which the aging could be neglected (loss of permeability less than 1% per week). For PIM-1, this occurs after 102 days and for PIM-EA-TB after 214 days. The expected permeability at these times were $4.5 \cdot 10^4$ Barrer for PIM-1 and $2.0 \cdot 10^4$ Barrer for PIM-EA-TB. In comparison with the maximum permeability, this means a loss of the initial permeability of 55% for PIM-1 and of 80% for PIM-EA-TB.

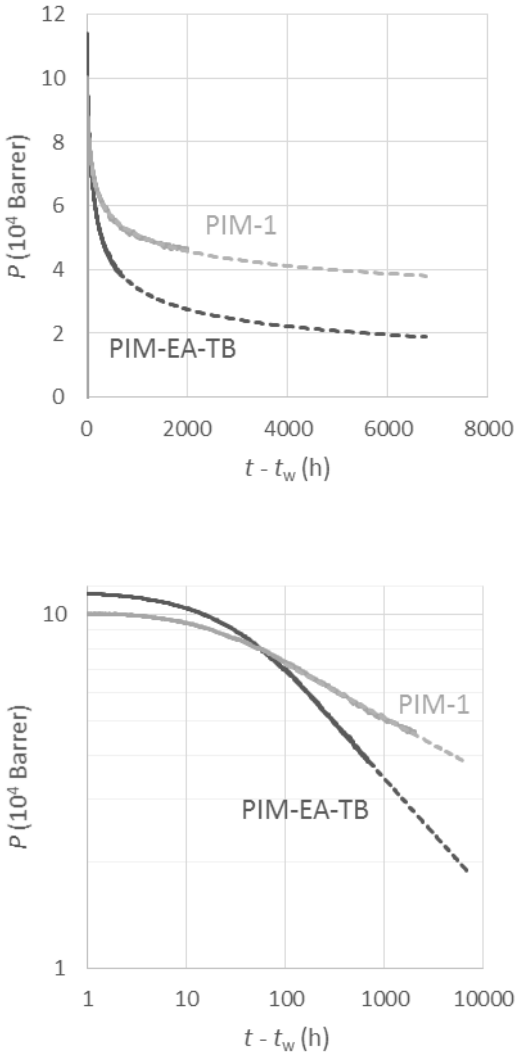

Figure 11 – Prediction of permeability decline using Eq. (2) in linear (upper plot) and log-log (lower plot) scale. The solid line represents the experimental behaviour and the dashed line the predicted behaviour. Both plots show the same data.

4 Conclusion

For the first time, we provide an evidence that aging of both PIM-1 and PIM-EA-TB is mostly of a physical nature. Using the theory from analogical rheological studies, we show that the aging in continuous mode of permeability measurement was *faster* than in the momentary mode. This was probably caused by the permanent presence of MeOH inside the tested membrane during the

continuous measurement, thus causing an additional contribution to aging. In this case, MeOH seems to increase the mobility of polymeric chains, allowing them to pack more rapidly. In general, our findings show that all aging measurements should be carried out with special care and preferably in the continuous mode of measurement or, at least, in such a way that it is possible to predict the continuous, industrially interesting, behaviour. From the very high correlation coefficients between diffusion and permeation coefficients, we suggest that the aging process of PIMs is predominately influenced by the decrease of diffusion coefficient. This could possibly be caused by the decrease of the mobility of polymer chains over time. The less mobile chains then block the penetrants path and thus lower the diffusion coefficient, while the sorption capacity stay at the same level. After all, the determined findings can improve the knowledge of the aging phenomenon in the glassy high free volume polymers and contribute to the improvement of aging predictions for PIMs and potentially for other glassy polymers.

Acknowledgement

Parts of the work leading to these results have received funding from the European Community's Seventh Framework Programme (FP7/2007-2013) under grant agreement no. NMP3-SL-2009-228631, project DoubleNanoMem. The financial support of the Czech Science Foundation (Grant No. P106/10/1194 and 13-32829P) and financial support from specific university research (MSMT No 20/2015) is greatly acknowledged. PIM-1 was sythesised by Louise Maynard-Atem, funded by EPSRC research grant EP/G065144/1. The authors are also thankful for the help of Professor Petr Sysel (Department of Polymers, University of Chemistry and Technology Prague).

References

[1] N.B. McKeown, P.M. Budd, K.J. Msayib, B.S. Ghanem, H.J. Kingston, C.E. Tattershall, S.M. Makhseed, K. Reynolds, D. Fritsch, Polymers of intrinsic microporosity (PIMs): bridging the void between microporous and polymeric materials, Chemistry, 11 (2005) 2610-2620.
[2] L.M. Robeson, The upper bound revisited, Journal of Membrane Science, 320 (2008) 390-400.
[3] P.M. Budd, N.B. McKeown, B.S. Ghanem, K.J. Msayib, D. Fritsch, L. Starannikova, N. Belov, O. Sanfirova, Y. Yampolskii, V. Shantarovich, Gas permeation parameters and other physicochemical properties of a polymer of intrinsic microporosity: Polybenzodioxane PIM-1, Journal of Membrane Science, 325 (2008) 851-860.
[4] A.F. Bushell, M.P. Attfield, C.R. Mason, P.M. Budd, Y. Yampolskii, L. Starannikova, A. Rebrov, F. Bazzarelli, P. Bernardo, J.C. Jansen, M. Lanc, K. Friess, V. Shantarovich, V. Gustov, V. Isaeva, Gas permeation parameters of mixed matrix membranes based on the polymer of intrinsic microporosity PIM-1 and the zeolitic imidazolate framework ZIF-8, Journal of Membrane Science, 427 (2013) 48-62.
[5] M. Carta, R. Malpass-Evans, M. Croad, Y. Rogan, J.C. Jansen, P. Bernardo, F. Bazzarelli, N.B. McKeown, An Efficient Polymer Molecular Sieve for Membrane Gas Separations, Science, 339 (2013) 303-307.

[6] E. Tocci, L. De Lorenzo, P. Bernardo, G. Clarizia, F. Bazzarelli, N.B. McKeown, M. Carta, R. Malpass-Evans, K. Friess, K. Pilnáček, M. Lanč, Y.P. Yampolskii, L. Strarannikova, V. Shantarovich, M. Mauri, J.C. Jansen, Molecular Modeling and Gas Permeation Properties of a Polymer of Intrinsic Microporosity Composed of Ethanoanthracene and Tröger's Base Units, Macromolecules, 47 (2014) 7900-7916.
[7] O. Vopička, K. Friess, V. Hynek, P. Sysel, M. Zgazar, M. Sipek, K. Pilnáček, M. Lanc, J.C. Jansen, C.R. Mason, P.M. Budd, Equilibrium and transient sorption of vapours and gases in the polymer of intrinsic microporosity PIM-1, Journal of Membrane Science, 434 (2013) 148-160.
[8] P.H. Pfromm, The Impact of Physical Aging of Amorphous Glassy Polymers on Gas Separation Membranes, in: Materials Science of Membranes for Gas and Vapor Separation, John Wiley & Sons, Ltd, 2006, pp. 293-306.
[9] S. Harms, K. Rätzke, F. Faupel, N. Chaukura, P.M. Budd, W. Egger, L. Ravelli, Aging and Free Volume in a Polymer of Intrinsic Microporosity (PIM-1), The Journal of Adhesion, 88 (2012) 608-619.
[10] F.Y. Li, T.-S. Chung, Physical aging, high temperature and water vapor permeation studies of UV-rearranged PIM-1 membranes for advanced hydrogen purification and production, International Journal of Hydrogen Energy, 38 (2013) 9786-9793.
[11] C.L. Staiger, S.J. Pas, A.J. Hill, C.J. Cornelius, Gas Separation, Free Volume Distribution, and Physical Aging of a Highly Microporous Spirobisindane Polymer, Chemistry of Materials, 20 (2008) 2606-2608.
[12] A.G. McDermott, P.M. Budd, N.B. McKeown, C.M. Colina, J. Runt, Physical aging of polymers of intrinsic microporosity: a SAXS/WAXS study, Journal of Materials Chemistry A, 2 (2014) 11742-11752.
[13] X.-Y. Wang, F.T. Willmore, R.D. Raharjo, X. Wang, B.D. Freeman, A.J. Hill, I.C. Sanchez, Molecular Simulations of Physical Aging in Polymer Membrane Materials, The Journal of Physical Chemistry B, 110 (2006) 16685-16693.
[14] T.P. Witelski, Traveling wave solutions for case II diffusion in polymers, Journal of Polymer Science Part B Polymer Physics, 34 (1996) 141-150.
[15] N.L. Thomas, A.H. Windle, A theory of case II diffusion, Polymer, 23 (1982) 529-542.
[16] J.H. Petropoulos, M. Sanopoulou, K.G. Papadokostaki, Physically insightful modeling of non-Fickian kinetic regimes encountered in fundamental studies of isothermal sorption of swelling agents in polymeric media, European Polymer Journal, 47 (2011) 2053-2062.
[17] P.K. Vijalapura, S. Govindjee, Numerical simulation of coupled-stress case II diffusion in one dimension, Journal of Polymer Science Part B: Polymer Physics, 41 (2003) 2091-2108.
[18] J. Vrentas, C. Vrentas, Viscoelastic diffusion, Journal of Polymer Science Part B: Polymer Physics, 39 (2001) 1529-1547.
[19] M.R. Shah, R.D. Noble, D.E. Clough, Analysis of transient permeation as a technique for determination of sorption and diffusion in supported membranes, Journal of Membrane Science, 280 (2006) 452-460.
[20] O. Vopička, V. Hynek, V. Rabová, Measuring the transient diffusion of vapor mixtures through dense membranes, Journal of Membrane Science, 350 (2010) 217-225.
[21] C.Y. Zeng, J.D. Li, P. Li, T.Q. Chen, Y.Z. Lin, D. Wang, C.X. Chen, A novel transport model for sorption and desorption of penetrants in dense polymeric membranes, Chemical Engineering Science, 61 (2006) 1892-1900.
[22] T.L. Hill, G. Scatchard, B.A. Pethica, I.J. Straub, R. SchloGl, G. Manecke, R. SchloGl, M. Nagasawa, I. Kagawa, P. Meares, K. Sollner, F.L. Tye, A. Despia, G.J. Hills, F. Helfferich, R.J.P. Williams, A.M. Peers, F. Bergsma, A.J. Staverman, N. Krishnaswamy, F. Runge, F. Wolf, E. Glueckauf, D. Reichenberg, R. Neihof, R.D. Keynes, A.R. Ubbelohde, R.M. Barrer, General discussion, Discussions of the Faraday Society, 21 (1956) 117-140.
[23] M. Kitchin, J. Teo, K. Konstas, C.H. Lau, C.J. Sumby, A.W. Thornton, C.J. Doonan, M.R. Hill, AIMs: a new strategy to control physical aging and gas transport in mixed-matrix membranes, Journal of Materials Chemistry A, 3 (2015) 15241-15247.
[24] C.H. Lau, K. Konstas, A.W. Thornton, A.C.Y. Liu, S. Mudie, D.F. Kennedy, S.C. Howard, A.J. Hill, M.R. Hill, Gas-Separation Membranes Loaded with Porous Aromatic Frameworks that Improve with Age, Angewandte Chemie International Edition, 54 (2015) 2669-2673.

[25] C.H. Lau, P.T. Nguyen, M.R. Hill, A.W. Thornton, K. Konstas, C.M. Doherty, R.J. Mulder, L. Bourgeois, A.C.Y. Liu, D.J. Sprouster, J.P. Sullivan, T.J. Bastow, A.J. Hill, D.L. Gin, R.D. Noble, Ending Aging in Super Glassy Polymer Membranes, Angewandte Chemie International Edition, 53 (2014) 5322-5326.
[26] A.F. Bushell, P.M. Budd, M.P. Attfield, J.T.A. Jones, T. Hasell, A.I. Cooper, P. Bernardo, F. Bazzarelli, G. Clarizia, J.C. Jansen, Nanoporous Organic Polymer/Cage Composite Membranes, Angewandte Chemie International Edition, 52 (2013) 1253-1256.
[27] T. Mitra, R.S. Bhavsar, D.J. Adams, P.M. Budd, A.I. Cooper, PIM-1 mixed matrix membranes for gas separations using cost-effective hypercrosslinked nanoparticle fillers, Chem Commun (Camb), (2016).
[28] J.T.A. Jones, T. Hasell, X. Wu, J. Bacsa, K.E. Jelfs, M. Schmidtmann, S.Y. Chong, D.J. Adams, A. Trewin, F. Schiffman, F. Cora, B. Slater, A. Steiner, G.M. Day, A.I. Cooper, Modular and predictable assembly of porous organic molecular crystals, Nature, 474 (2011) 367-371.
[29] T. Ben, H. Ren, S. Ma, D. Cao, J. Lan, X. Jing, W. Wang, J. Xu, F. Deng, J.M. Simmons, S. Qiu, G. Zhu, Targeted Synthesis of a Porous Aromatic Framework with High Stability and Exceptionally High Surface Area, Angewandte Chemie, 121 (2009) 9621-9624.
[30] B.W. Rowe, S.J. Pas, A.J. Hill, R. Suzuki, B.D. Freeman, D.R. Paul, A variable energy positron annihilation lifetime spectroscopy study of physical aging in thin glassy polymer films, Polymer, 50 (2009) 6149-6156.
[31] Y. Huang, D.R. Paul, Physical aging of thin glassy polymer films monitored by gas permeability, Polymer, 45 (2004) 8377-8393.
[32] M. McCaig, D.R. Paul, Effect of film thickness on the changes in gas permeability of a glassy polyarylate due to physical agingPart I. Experimental observations, Polymer, 41 (2000) 629-637.
[33] P.M. Budd, B.S. Ghanem, S.M. Makhseed, N.B. McKeown, K.J. Msayib, C.E. Tattershall, Polymers of intrinsic microporosity (PIMs): robust, solution-processable, organic nanoporous materials, Chem Commun (Camb), (2004) 230-231.
[34] M. Heuchel, D. Fritsch, P.M. Budd, N.B. McKeown, D. Hofmann, Atomistic packing model and free volume distribution of a polymer with intrinsic microporosity (PIM-1), Journal of Membrane Science, 318 (2008) 84-99.
[35] H. Frentrup, K.E. Hart, C.M. Colina, E.A. Muller, In Silico Determination of Gas Permeabilities by Non-Equilibrium Molecular Dynamics: CO2 and He through PIM-1, Membranes, 5 (2015) 99-119.
[36] L.C.E. Struik, Physical aging in amorphous polymers and other materials, Elsevier Amsterdam, 1978.
[37] A. Shanhin, Y.M. Joshi, Prediction of Long and Short Time Rheological Behavior in Soft Glassy Materials, Physical Review Letters, 106 (2011).
[38] Y.M. Joshi, Long time response of aging glassy polymers, Rheol Acta, 53 (2014) 477-488.
[39] G.B. McKenna, A.J. Kovacs, Physical aging of poly(methyl methacrylate) in the nonlinear range: Torque and normal force measurements, Polymer Engineering & Science, 24 (1984) 1138-1141.
[40] L. Guerdoux, R.A. Duckett, D. Froelich, Physical ageing of polycarbonate and PMMA by dynamic mechanical measurements, Polymer, 25 (1984) 1392-1396.
[41] C. Zhou, T.S. Chung, R. Wang, S. Hong Goh, A governing equation for physical aging of thick and thin fluoropolyimide films, Journal of applied polymer science, 92 (2004) 1758-1764.
[42] M. Carta, R. Malpass-Evans, M. Croad, Y. Rogan, M. Lee, I. Rose, N.B. McKeown, The synthesis of microporous polymers using Troger's base formation, Polymer Chemistry, 5 (2014) 5267-5272.
[43] P.M. Budd, E.S. Elabas, B.S. Ghanem, S. Makhseed, N.B. McKeown, K.J. Msayib, C.E. Tattershall, D. Wang, Solution-processed, organophilic membrane derived from a polymer of intrinsic microporosity, Advanced Materials, 16 (2004) 456-+.
[44] L. Hendrich, V. Hynek, M. Šípek, Diferenciální permeametr určený k měření propustnosti plynů a par organických látek skrze ploché polymerní membrány, Chem. Listy, 99 (2005) 345-350.
[45] K. Friess, M. Šípek, V. Hynek, P. Sysel, K. Bohatá, P. Izák, Comparison of permeability coefficients of organic vapors through non-porous polymer membranes by two different experimental techniques, Journal of Membrane Science, 240 (2004) 179-185.

[46] K. Pilnáček, M. Šípek, O. Vopička, K. Friess, Experimentální stanovení transportních parametrů plynů a par, in: M. Šípek (Ed.) Membránové dělení plynů a par, University of Chemistry and Technology in Prague, Prague, 2014, pp. 75-102.
[47] O. Vopička, D. Radotínský, K. Friess, Sorption of vapour mixtures of methanol and dimethyl carbonate in PDMS: Experimental study, European Polymer Journal, 73 (2015) 480-486.
[48] E.A. Guggenheim, Applications of statistical mechanics, Clarendon press Oxford, 1966.
[49] R.B. Anderson, Modifications of the Brunauer, Emmett and Teller Equation1, Journal of the American Chemical Society, 68 (1946) 686-691.
[50] J.H. Boer, Dynamical character of adsorption, (1968).
[51] A. Heintz, W. Stephan, A generalized solution—diffusion model of the pervaporation process through composite membranes Part II. Concentration polarization, coupled diffusion and the influence of the porous support layer, Journal of Membrane Science, 89 (1994) 153-169.
[52] J. Crank, The mathematics of diffusion, Clarendon Press, Oxford, 1975.
[53] C. Analytics, Anaconda Software Distribution., in, Continuum Analytics, pp. Computer software.
[54] C. Andersson, C. Führer, J. Åkesson, Assimulo: A unified framework for ODE solvers, Mathematics and Computers in Simulation, 116 (2015) 26-43.
[55] M. Newville, T. Stensitzki, D.B. Allen, A. Ingargiola, LMFIT: Non-Linear Least-Square Minimization and Curve-Fitting for Python, Zenodo, (2014).
[56] P. Bernardo, F. Bazzarelli, F. Tasselli, G. Clarizia, C.R. Mason, L. Maynard-Atem, P.M. Budd, K. Friess, M. Lanč, O. Vopicka, K. Pilnáček, D. Fritsch, Y. Yampolskii, V. Shantarovich, J.C. Jansen, Effect of physical aging on the gas transport and sorption in PIM-1 membranes, in preparation, (2017).
[57] R. Swaidan, B. Ghanem, E. Litwiller, I. Pinnau, Physical Aging, Plasticization and Their Effects on Gas Permeation in “Rigid” Polymers of Intrinsic Microporosity, Macromolecules, (2015).
[58] S. Thomas, I. Pinnau, N. Du, M.D. Guiver, Pure- and mixed-gas permeation properties of a microporous spirobisindane-based ladder polymer (PIM-1), Journal of Membrane Science, 333 (2009) 125-131.
[59] Y. Yampolskii, A. Alentiev, G. Bondarenko, Y. Kostina, M. Heuchel, Intermolecular Interactions: New Way to Govern Transport Properties of Membrane Materials, Ind Eng Chem Res, 49 (2010) 12031-12037.
[60] R. Taylor, R. Krishna, Multicomponent mass transfer, John Wiley & Sons, 1993.

A Appendix

A.1 Derivation of thermodynamic Fick’s law

In this section, the background of thermodynamic Fick’s diffusion flux based on irreversible thermodynamics [60] is revealed. The starting point is the rate of entropy production per unit volume. For an isothermal, isobaric process in the absence of an external force field, the rate of one-dimensional entropy production due to diffusion is given by

$$-\left(\frac{\partial \mu}{\partial z}\right)_{T,p} \cdot J_{\mathrm{mol}} \geq 0 \qquad (15)$$

where J_{mol} is the molar diffusion flux with respect to the molar average reference velocity and $(\partial\mu/\partial z)$ is the chemical potential gradient, which may be interpreted as the driving force for diffusion. In the case of thermodynamic Fick's diffusion flux, a linear relationship between total flux and driving force is postulated as follows

$$c\left(\frac{\partial\mu}{\partial z}\right)_{T,p} = -H \cdot J_{\mathrm{mol}} \tag{16}$$

where H is a coefficient measuring the mobility of the diffusing molecules. Since the chemical potential and the activity of substance in the polymer are related by $\mu = \mu_{\mathrm{ref}} + RT\ln a$, equation (16) can be rewritten as follows

$$J_{\mathrm{mol}} = -c\mathfrak{D}\frac{\mathrm{d}\ln a}{\mathrm{d}c}\frac{\mathrm{d}c}{\mathrm{d}z}$$

where $\mathfrak{D} = RT/H$ is the thermodynamic diffusion coefficient. If the diffusing substance has a constant value of density and the system meets the Amagat's law, then the amount of penetrant can be expressed by the volume fraction instead of molar concentration, hence

$$J_{\mathrm{vol}} = -\mathfrak{D} \cdot \left(\phi\frac{\partial\ln a}{\partial\phi}\right)\frac{\mathrm{d}\phi}{\mathrm{d}z} \tag{17}$$

A.2 Methanol treatment

To the best of our knowledge, the removal of residual solvent (chloroform) was studied only for PIM-EA-TB (see the literature [6]). Hence, in order to have a complete picture, we provide transmission IR spectra of as-cast and MeOH treated PIM-1 membrane.

The most intensive vibration modes characteristic for chloroform are usually at *ca*. 3020, 1216, 760 and 670 cm^{-1}. In the spectrum of PIM-1 as-cast we observed these bands at 3026, 757 and 669 cm^{-1} (grey spectrum in Figure A.1). In an average spectrum of a membrane after the MeOH treatment, chloroform bands were reduced (for details see Figure A.1). The bands at 3026 and 669 cm^{-1} were minimized completely and the width of the band at 757 cm^{-1} decreased because of the disappearance of chloroform. This indicates very strong, if not complete, removal of the residual solvent.

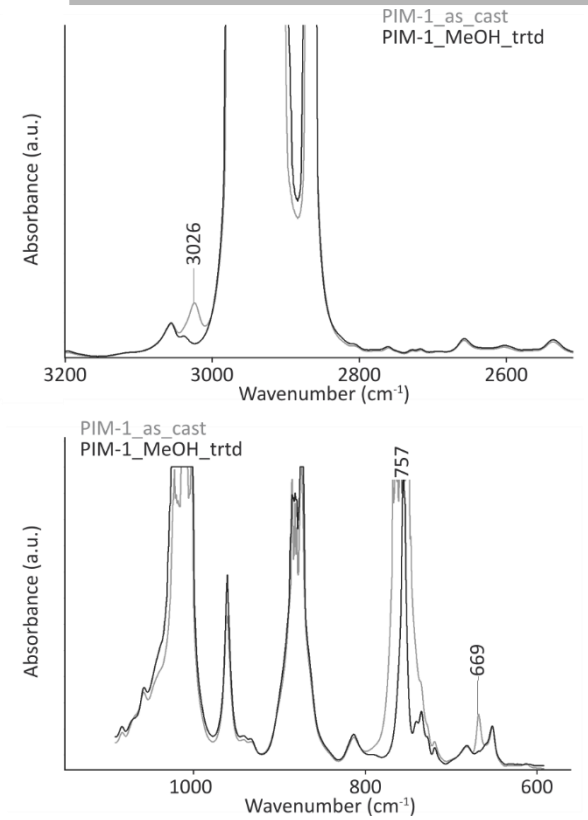

Figure A.1 – Comparison of cut-offs of IR transmission spectra of as-cast (grey line) and MeOH treated (black line) PIM-1 membrane.

A.3 Transport coefficients

Table A.1 – Permeabilities and diffusivities of momentary experiments (MeOH activity 0.2) on PIM-1. The data are shown in Figure 7 (upper). The crossed out values were not included in correlations.

t_w (h)	P (10^4 Barrer)	α Eq. (13)	D Eq. (9) (10^{-12} m^2/s)	adj. R^2 Eq. (9)	$\mathfrak{D}$ Eq. (6) (10^{-12} m^2/s)	adj. R^2 Eq. (6)
3	~~9.8~~	1.00	~~16.2~~	0.997	~~13.7~~	0.991
27	8.4	0.97	13.7	0.998	11.6	0.993
99	7.8	0.89	12.1	0.986	10.2	0.978
125	6.7	0.99	11.8	0.997	9.9	0.992
146	6.6	0.98	11.3	0.997	9.5	0.991
194	6.4	0.95	11.2	0.999	9.3	0.995
267	6.3	0.93	10.1	0.986	8.6	0.979
314	5.9	0.94	9.5	0.991	8.0	0.984
362	5.4	1.02	9.7	0.992	8.1	0.987
438	5.4	1.01	9.4	0.997	7.9	0.992
458	5.2	1.04	9.2	0.997	7.7	0.990
484	5.1	1.05	9.2	0.998	7.7	0.992
531	5.4	0.98	8.7	0.997	7.3	0.992
603	5.1	1.00	8.8	0.997	7.3	0.991
795	5.1	~~0.95~~	8.3	0.995	6.9	0.988
939	4.7	~~0.99~~	8.2	0.993	6.9	0.986
1179	4.6	~~0.98~~	8.4	0.998	7.0	0.992
1275	4.7	0.95	8.1	0.996	6.8	0.992

2835	4.6	~~0.85~~	7.9	0.998	6.6	0.992

Table A.2 – Permeabilities and diffusivities of momentary experiments (MeOH activity 0.2) on PIM-EA-TB. The data are shown in Figure 7 (lower). The crossed out values were not included in correlations.

t_w (h)	P (10^4 Barrer)	α Eq. (13)	D Eq. (9) (10^{-12} m^2/s)	adj. R^2 Eq. (9)	$\mathfrak{D}$ Eq. (6) (10^{-12} m^2/s)	adj. R^2 Eq. (6)
27	3.3	1.00	5.3	0.989	3.9	0.998
31	3.0	1.08	5.0	0.988	3.7	0.998
52	2.9	1.02	4.1	0.991	3.0	0.999
55	2.8	1.04	4.5	0.991	3.3	0.999
123	2.6	0.95	3.9	0.992	2.8	0.999
147	2.7	0.87	3.9	0.989	2.9	0.999
172	2.4	0.92	3.9	0.991	2.8	0.999
196	2.3	0.91	3.7	0.992	2.6	0.999
220	2.4	0.88	3.4	0.993	2.6	0.999
292	2.3	0.84	3.6	0.987	2.6	0.998
315	2.0	0.94	3.3	0.993	2.4	0.999
339	2.2	0.85	3.3	0.992	2.3	0.998
362	2.1	0.87	3.1	0.995	2.3	0.999
391	2.0	0.87	3.0	0.995	2.2	0.999
459	2.0	0.85	3.2	0.991	2.3	0.999
483	1.9	0.87	3.2	0.991	2.3	0.999
508	1.7	0.94	3.0	0.992	2.2	0.998
530	1.9	0.87	3.2	0.990	2.2	0.999
555	1.8	0.87	2.9	0.996	2.1	0.999
628	1.8	0.83	2.9	0.994	2.1	0.998
653	1.8	0.84	2.8	0.993	2.0	0.998
677	1.6	0.90	2.7	0.996	1.9	0.998
700	1.6	0.91	2.7	0.997	1.9	0.996
725	1.6	0.91	2.6	0.996	1.9	0.998
795	1.7	0.84	2.7	0.996	2.0	0.999
819	1.6	0.88	2.5	0.994	1.8	0.998
3	13.3	~~0.32~~	9.6	1.000	7.7	0.996

A.4 Sorption data

Table A.3 – Sorption of MeOH in PIM-EA-TB.

t_w (h)	p/p^{sat} (-)	w (-)
3	0.198	0.173
7	0.147	0.153
26	0.053	0.103
31	0.098	0.132
51	0.310	0.199
74	0.418	0.224
147	0.634	0.272
171	0.802	0.316

175	0.879	0.338
196	0.202	0.175

Highlights

- For the first time, we show continuous aging experiments
- PIM-1 and PIM-EA-TB undergo mostly physical aging, no chemical changes were detected
- Aging rate is the highest for permeation operated continuously
- Aging is driven by the decrease in diffusion coefficient
- Aging during the continuous permeation was successfully predicted from momentary experiments

Graphical abstract